Variable diffusion and conductivity change in 3D rotating Williamson fluid flow along with magnetic field and activation energy

Mair Khan
Department of Mathematics, Quaid-I-Azam University, Islamabad, Pakistan

T. Salahuddin
Department of Mathematics, Faculty of Science, Mirpur University of Science and Technology, Mirpur, Pakistan

Muhammad Malik Yousaf
Department of Mathematics, College of Sciences, King Khalid University, Abha, Saudi Arabia, and

Farzana Khan and Arif Hussain
Department of Mathematics, Quaid-I-Azam University, Islamabad, Pakistan

Received 22 February 2019
Revised 1 April 2019
Accepted 22 April 2019

Abstract

Purpose – The purpose of the current flow configurations is to bring to attention the thermophysical aspects of magnetohydrodynamics (MHD) Williamson nanofluid flow under the effects of Joule heating, nonlinear thermal radiation, variable thermal coefficient and activation energy past a rotating stretchable surface.

Design/methodology/approach – A mathematical model is examined to study the heat and mass transport analysis of steady MHD Williamson fluid flow past a rotating stretchable surface. Impact of activation energy with newly introduced variable diffusion coefficient at the mass equation is considered. The transport phenomenon is modeled by using highly nonlinear PDEs which are then reduced into dimensionless form by using similarity transformation. The resulting equations are then solved with the aid of fifth-order Fehlberg method.

Findings – The rotating fluid, heat and mass transport effects are analyzed for different values of parameters on velocity, energy and diffusion distributions. Parameters like the rotation parameter, Hartmann number and Weissenberg number control the flow field. In addition, the solar radiation, Joule heating, Prandtl number, thermal conductivity, concentration diffusion coefficient and activation energy control the temperature and concentration profiles inside the stretching surface. It can be analyzed that for higher values of thermal conductivity, Eckret number and solar radiation parameter the temperature

The authors extend their appreciation to the Deanship of Scientific Research at King Khalid University, Abha 61413, Saudi Arabia for funding this work through research groups program under grant number R.G.P-2/29/40.

Conflict of interest: The corresponding author on behalf of all authors declares "no conflict of interest".

International Journal of Numerical Methods for Heat & Fluid Flow
Vol. 30 No. 5, 2020
pp. 2467-2484
Emerald Publishing Limited
0961-5539
DOI 10.1108/HFF-02-2019-0145

profile increases, whereas opposite behavior is noticed for Prandtl number. Moreover, for increasing values of temperature difference parameter and thermal diffusion coefficient, the concentration profile shows reducing behavior.

Originality/value – This paper is useful for researchers working in mathematical and theoretical physics. Moreover, numerical results are very useful in industry and daily-use processes.

Keywords Magnetic field, Shooting method, Solar radiation, Joule heating, Activation energy, Williamson fluid, Variable diffusion coefficient

Paper type Research paper

1. Introduction

The study of heat and mass transfer is very beneficial due to its practical applications in engineering, ground water pollution, temperature controlled reactor, geophysical, electrical machinery, flat-plate solar collector, microelectronic device, thermal insulation buildings, etc. (Jonnadulaa *et al.*, 2015) demonstrated heat and mass transfer characteristics of chemical reaction on magnetohydrodynamics (MHD) flow induced by a permeable stretching surface. The transformed equations were solved by using an effective numerical scheme known as implicit finite difference scheme. Pal and Mandal, (2017) exemplified the magnetic field of heat and mass transport close a stagnation point due to a shrinking/stretching sheet. Mishra and Bhatti (2017) analyzed chemical response on heat and mass assignment flow induced by a linear stretching surface with Ohmic heating. The thermal and concentration diffusions in nanofluid flow due to linear and nonlinear stretching surface was presented by Sreedevi *et al.* (Eid and Mahny, 2017). Sui *et al.* (2018) discussed the unsteady heat and mass transfer non-Newtonian nanoliquid flow over a permeable stretching surface. It was found that the concentration and thermal boundary layer becomes large foe higher values of heat generation and magnetic field. Sui *et al.* Khan *et al.* (2018a) analyzed heat and mass transfer micropolar fluid over a stretching surface along with slip effect. Khan *et al.* Gireesha *et al.* (2018) deliberated the effects of heat and mass transfer on Williamson nanofluid induced by a nonlinear stretching surface. Viscosity was assumed to be temperature dependent. Gireesha *et al.* Khan *et al.* (2018b) performed the thermal and concentration diffusions in Oldroyed-B nanofluid flow due to a stretching surface with convective boundary condition. It was found that concentration profile diminishes for improving values of Lewis number. Khan *et al.* Sarojamma *et al.* (2018) analyzed heat and mass diffusion in Jeffery nanofluid flow persuaded by inclined stretching sheet in the presences of magnetic field. Sarojamma *et al.* Azizian *et al.* (2014) discussed the thermal and solutal stratification effects in non-Newtonian micropolar fluid flow due to stretched sheet along with transport of heat energy and mass species.

The work on MHD for electrical conducting fluid due to a heat surface has increased great attention of numerous researchers in view of its significant applications in several problems such as petroleum industries, plasma study, glass manufacturing, cooling of nuclear reactors and crystal growth. The impact of external magnetic field on heat diffusion coefficient of magnetite nanoliquid in laminar flow regime was presented by Azizian *et al.* (Makinde *et al.*, 2016). Sreedevi *et al.* (2017) presented the concept of variable viscosity on MHD nanofluid flow due to a radially stretched surface. Khan *et al.* (2017) exemplified the chemical reaction change in concentration diffusion on MHD Williamson nanofluid flow due to an isothermal cone and plate in preamble surface. Joule heating was also considered in heat equation. Nourazar *et al.* (2017) investigated the MHD flow of nanofluid induced by a preamble stretching cylinder and calculated the solution by Optimal collection scheme. Ramay *et al.* (2018) investigated the effect of thermal wall slip on MHD nanofluids flow over

a nonlinear stretching surface. Turkyilmazoglu (2018) illustrated the effect of magnetohydrodynamic viscous fluid over a nonlinearly deforming porous surface. (Chen *et al.*, 2018) examined the hydromagnetic flow of a viscoelastic fluid induced by a stretching surface.

In fluid mechanics, fluid is divided into three classes, namely, integral type, differential type and rate type. The Williamson fluid is one of the simplest model that describes the characteristics of pseudoplastic materials. This model was presented by (Williamson, 1929). Nadeem *et al.* (2013) investigated the two-dimensional boundary layer equations for Williamson liquid induced by a stretching surface. Kumaran and Sandeep (2017) exemplified the heat and mass diffusions in magnetohydrodynamic Casson and Williamson fluid flow due to a parboiled surface. It was seen that mass and heat transfer in Casson fluid was comparatively large than that of Williamson fluid. Khan *et al.* (2018c) discussed the computational aspect of temperature based variable viscosity on Williamson nanoliquid over a nonlinear stretching surface. Soomro *et al.* (2018) analyzed the numerical simulation of MHD stagnation point flow on Williamson nanoliquid due to a vertical moving surface. Temperature and concentration of nanoliquid was reduced due to increase in thermal and solutal slip parameters. Some recent literature to relevant of nanofluid flow are illustrated **(**Farooq *et al.*, 2018**;** Hayat *et al.*, 2016a**;** Hayat *et al.*, 2015**;** Khan *et al.*, 2018d**;** Khan *et al.*, 2018e**;** Hayat *et al.*, 2016b**).**

In the current article, the main objective is to examine the transport of MHD Williamson fluid flow over an accelerated/decelerated rotating stretchable surface along with heat and mass diffusions. The modeling includes the similarity transformations in order to convert the partial differential equations into ordinary differential equations and then the problem is solved by numerically by fifth order RK-Fehlberg technique. Graphs and tables are constructed in order to examine the velocity, heat and mass diffusions for different values of dimensionless parameters.

2. Mathematical formulation

2.1 Flow formulation

Let us assume the variable diffusion coefficients (mass diffusion coefficient and thermal conductivity) in Williamson rotating incompressible fluid flow due to elastic stretching surface placed in xy–plane, where fluid is positioned at $z \geq 0$. It is assumed that the surface is stretched with velocity $u_w = cx$ in x–direction, where $c > 0$. Let C_w and T_w be the concentration and temperature at the surface. Therefore, C_∞ and T_∞ are the concentration and temperature far away from the surface as illustrated in Figure 1. The solar radiation and Joule heating are added in the problem. In addition, the magnetic field H_o is applied perpendicular to the stretched plan.

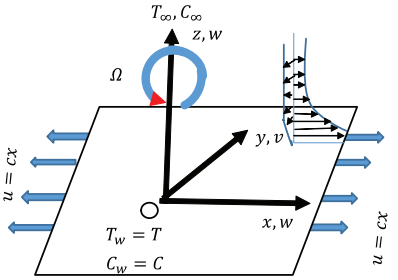

Figure 1.
Geometry of the problem

2.2 Rheological model for Williamson model

Cauchy stress tensor for Williamson fluid model is defined as:

$$\mathbf{S}^* = -P\mathbf{I} + \boldsymbol{\tau}, \tag{1}$$

$$\boldsymbol{\tau} = \left(\mu_\infty + \frac{\mu_0 - \mu_\infty}{1 - \Gamma \overset{o}{\gamma}}\right)\mathbf{A}_1, \tag{2}$$

where:

$$\overset{o}{\gamma} = \sqrt{\frac{1}{2}\pi}, \ \pi = tra\left(\mathbf{A}_1^2\right), \tag{3}$$

in which $\mathbf{S}^*$ is the extra tensor, I is the identity tensor, P is the Hydrostatic pressure, τ is the Cauchy tensor, μ_0 denotes limiting viscosity at zero shear rate, μ_∞ represents limiting at infinite shear rate, $\Gamma > 0$ is a time constant, $\mathbf{A}_1 = (\nabla V^*) + (\nabla V^*)^t = L + L^t$ is the first Rivlin–Erkicsen tensor.

We assume that $\mu_\infty = 0$ and $\Gamma \overset{o}{\gamma} < 1$. equation (2) becomes:

$$\boldsymbol{\tau} = \left(\frac{\mu_0}{1 - \Gamma \overset{o}{\gamma}}\right)\mathbf{A}_{1,} \tag{4}$$

using binomial expansion we get:

$$\boldsymbol{\tau} = \mu_0\left(1 + \Gamma \overset{o}{\gamma}\right)\mathbf{A}_{1,} \tag{5}$$

2.3 Binary chemical reaction and activation energy

Fist order chemical reaction and activation energy are:

$$K_A^* = K_B^*\left(\frac{T}{T_\infty}\right)^n \exp\left[\frac{-E_a}{kT}\right], \tag{6}$$

where K_A^* denotes the rate of chemical reaction $\left(\frac{1}{\sec}\right)$, E_a is the activation energy (eV), K_B^* represents the pre-exponential constant $\left(\frac{K^{-n}}{\sec}\right)$, n is the fitted rate constant lies in the range $-1 < n < 1$, T_0 is known as reference temperature, the expression $K_B^*\left(\frac{T}{T_\infty}\right)^n \exp\left[\frac{-E_a}{kT}\right]$ denotes the modified Arrhenius function and $k = 8.61 \times 10^{-5}$ denotes the Boltzmann constant $\left(\frac{eV}{K}\right)$.

2.4 Problem formulation

Basic equations of heat and mass transfer 3 D Williamson rotating fluid flow are

2.4.1 Continuity equation

$$\text{div } V^* = 0, \tag{7}$$

continuity equation can be written in component form

$$\partial_x u + \partial_y v + \partial_z w = 0, \tag{8}$$

2.4.2 Momentum equation

$$\rho \frac{dV}{dt}(\Omega \times \Omega \times r) + (2\Omega \times V) = -\nabla P + \operatorname{div} \mathbf{S}^* + \mathbf{J} \times H_o, \tag{9}$$

where $\mathbf{J}$ is the current density, $H = [0, H_o, 0]$ is the external magnetic field, $\Omega = [0,0,\Omega]$ angular velocity and ∇ represents operator.

After boundary layer approximations, the Williamson model can be written as:

$$u\partial_x u + v\partial_y u + w\partial_z u - 2\Omega v = \partial_z\left(1 + \Gamma \overset{o}{\gamma}\right)\partial_z u - \frac{\sigma H_o^2}{\rho} u, \tag{10}$$

$$u\partial_x v + v\partial_y v + w\partial_z v - 2\Omega u = \partial_z\left(1 + \Gamma \overset{o}{\gamma}\right)\partial_z v - \frac{\sigma H_o^2}{\rho} v, \tag{11}$$

2.5 Variable diffusion coefficients

Studies considering temperature dependent linear thermal conductivity (Qureshi *et al.*, 2018) is:

$$K(T) = k_\infty \left[1 + \varepsilon_1 \left(\frac{T - T_\infty}{T_w - T_\infty}\right)\right], \tag{12}$$

here ε_1 is very small parameter. For $\varepsilon_1 = 0$ the above equation converts into constant thermal conductivity.

Now we consider the concentration diffusion coefficient as:

$$D(C) = k_\infty \left[1 + \varepsilon_2 \left(\frac{C - C_\infty}{C_w - C_\infty}\right)\right], \tag{13}$$

here ε_2 is very small parameter. Equation (13) is converted into constant mass diffusion coefficient for $\varepsilon_2 = 0$.

2.5.1 Energy and concentration equations

$$\frac{dT}{dt} = \frac{1}{(\rho c)_p} \nabla.(K(T)\nabla T) - \frac{1}{(\rho c)_p} \partial_z q_r + \frac{1}{(\rho c)_p} \frac{\sigma H_o^2}{\rho}(u^2 + v^2), \tag{14}$$

$$\frac{dC}{dt} = \nabla.\big(D(c)\nabla C\big) - K_A^*(C - C_\infty), \tag{15}$$

after applying the boundary layer approximations, energy and concentration equations become

$$u\partial_x T + v\partial_y T + w\partial_z T = \frac{k}{\rho c_p}\partial_z\left(K(T)\partial_z T\right) + \frac{1}{(\rho c)_p}\left(\frac{16T_\infty^3\sigma^*}{3k^*}\right)\partial_{zz}T + \frac{1}{(\rho c)_p}\frac{\sigma H_o^2}{\rho}(u^2+v^2), \tag{16}$$

$$u\partial_x C + v\partial_y C + w\partial_z C = \partial_z\left(D(T)\partial_z T\right) - K_B^*\left(\frac{T}{T_\infty}\right)^n \exp\left[\frac{-E_a}{kT}\right](C - C_\infty), \tag{17}$$

the specified boundary conditions are:

$$\begin{aligned} &u = U_w = cx,\ v = 0,\ T = T_w, C = C_w \text{ at } z = 0,\\ &u \to 0,\ v \to 0,\ T \to T_\infty, C \to C_\infty \text{ as } z \to \infty. \end{aligned} \tag{18}$$

Where ρ is the density, T_w is denotes temperature at the wall, σ is electrical conductivity of the liquid and c_p denotes the specific heat.

The main PDEs are reduced into ODEs by using following similarity transformations:

$$\begin{aligned} &u = cxf'(\eta),\ v = cxg(\eta),\ w = -\sqrt{c\nu}f(\eta),\ \eta = \sqrt{\frac{c}{\nu}}z,\\ &\theta(\eta)(T_w - T_\infty) = (T - T_\infty),\ \phi(\eta)(C_w - C_\infty) = (C - C_\infty). \end{aligned} \tag{19}$$

Continuity equation (8) is satisfied, while the boundary layer equations (10), (11), (16) and (17) are transformed into ODEs as:

$$Wef''\left(f''' + g''\right) + Wef''\left(\left(f'\right)^2 + \left(g'\right)^2\right) + \left(\sqrt{\left(f'\right)^2 + \left(g'\right)^2}\right)\left(f''' + f''f - \left(f'\right)^2 + 2\lambda g - Haf'\right) = 0, \tag{20}$$

$$Weg'\left(f''' + g''\right) + Weg''\left(\left(f'\right)^2 + \left(g'\right)^2\right) + \left(\sqrt{\left(f'\right)^2 + \left(g'\right)^2}\right)\left(g'' - f'g + g'f - 2\lambda f' - Hag\right) = 0, \tag{21}$$

$$\theta''(1 + \epsilon_1\theta + R) + \epsilon_1\left(\theta'\right)^2 + \Pr\theta' f + HaEc\Pr\left(f' + g\right) = 0, \tag{22}$$

$$\phi''(1 + \epsilon_2\phi) + \epsilon_2\left(\phi'\right)^2 + \Pr Lef\phi' - \Pr LeK(1 + \delta\theta)^n \exp\left[\frac{-E}{1 + \delta\theta}\right]\phi = 0, \tag{23}$$

Using equation (18), the boundary conditions become:

$$\begin{aligned} &\frac{df}{d\eta} = 1, f = 0, g = 0, \theta = 0, \phi = 1, \text{ at } \eta = 0, \\ &\frac{df}{d\eta} \to 0, \theta \to 0, \phi \to 0, as\ \eta \to \infty. \end{aligned} \tag{24}$$

where $\lambda = \frac{\Omega}{c}$ denotes the rotation parameter, $We = \Gamma cx\sqrt{\frac{\nu}{c}}$ is known as Weissenberg number, $Ha = \frac{\sigma H_o^2}{c\rho}$ represents the Hartmann number, $\Pr = \frac{\mu c_p}{k_\infty}$ is Prandtl number, $K = \frac{K_B^*}{c}$ denotes the dimensionless reaction rate, $E = \frac{E_a}{kT_\infty}$ represents the non-dimensional activation energy, $\delta = \frac{T_w - T_\infty}{T_\infty}$ is the temperature difference parameter, $Ec = \frac{U_w^2}{T_w - T_\infty}$ is the Eckert number, $Le = \frac{\nu}{D}$ is the Lewis number and $R = \frac{16\sigma^* T_\infty^3}{3k^* k_3}$ is thermal radiation parameter.

2.6 Physically interests

To get physical interests near the wall i.e. the friction factor coefficient, heat transfer rate and mass transfer rate, we use the following relations:

$$C_{f_x} = \frac{\tau_{xz}}{\rho U_w^2}, C_{f_y} = \frac{\tau_{yz}}{\rho U_w^2}, Nu = \frac{xq_w}{k(T_w - T_\infty)}, Sh = \frac{xJ_w}{k(C_w - C_\infty)}. \tag{25}$$

Here τ_w denotes the shear stress or skin friction, q_w and J_w denotes the heat and mass diffusion near the wall, where τ_{xz}, τ_{yz}, q_w and J_w are defined as:

$$\begin{aligned} \tau_{xz} &= \mu\left[\partial_z u + \left(\frac{\Gamma}{2}\sqrt{(\partial_z u)^2 + (\partial_z v)^2}\right)\partial_z u\right]_{z=0}, \\ \tau_{yz} &= \mu\left[\partial_z v + \left(\frac{\Gamma}{2}\sqrt{(\partial_z u)^2 + (\partial_z v)^2}\right)\partial_z v\right]_{z=0}, \\ q_w &= -K\left[\frac{\partial T}{\partial y}\right]_{z=0}, J_w = -D_b\left[\frac{\partial C}{\partial y}\right]_{z=0}. \end{aligned} \tag{26}$$

After using the scaling variables, friction factor, Nusselt and Sherwood numbers transformed into:

$$\begin{aligned} C_{f_x}\left(\mathrm{Re}_x^{\frac{1}{2}}\right) &= \left[f''(\eta) + Wef''(\eta)\sqrt{f''(\eta) + g'(\eta)}\right]_{\eta=0}, \\ C_{fy}\left(\mathrm{Re}_x^{\frac{1}{2}}\right) &= \left[g''(\eta) + Weg''(\eta)\sqrt{f''(\eta) + g'(\eta)}\right]_{\eta=0}, \\ Nu\mathrm{Re}_x^{\frac{-1}{2}} &= -\left(1 + \epsilon_1\theta(0) + R\right)\theta'(0),\ Sh\mathrm{Re}_x^{\frac{-1}{2}} = -\left(1 + \epsilon_2\phi(0)\right)\phi'(0). \end{aligned} \tag{27}$$

Where:

$$Re_x = \frac{U_w x}{\nu}.$$

3. Numerical procedure

In the procedure of numerical simulation, the technique used to solve the set of equations play an important role in view of its order and accuracy in yielding the solutions. A highly nonlinear differential equations (21)-(24) with corresponding boundary conditions (25) are solved using the RK-Fehlberg fifth order scheme along with Cash and Karp. The highly nonlinear ODEs are of 3rd order f, 2nd order θ and ϕ are then converted into simultaneous ordinary equations. With the initial conditions, we can take the values of $f'(\eta)$, $\theta(\eta)$, and $\phi(\eta)$. Thus, we may achieve unknown initial conditions at $\eta \to \infty$ using shooting method. The most important step of this technique is to choose the appropriate finite values of η. We choose $\eta_{\max} = 5$ which is adequate to obtain far field boundary conditions asymptotically for all values of the parameters considered.

4. Results and discussion

We expose the results to keep up the examine of various non-dimensional parameters such as Hartman number, activation energy, dimensionless reaction rate, thermal conductivity, mass diffusion coefficient and temperature difference parameter on velocity, skin friction coefficient, temperature, heat transfer rate, concentration and mass transfer rate. Figures 2 and 3 the radial and azimuthal velocity profiles for different values of *Ha*. It is found that the momentum flow field declines for increment values of Hartmann number *Ha*. This would happen because the application of transverse magnetic field sets Lorentz force, which retards the radial velocity. On the other hand, the azimuthal velocity profile is increased due to increase in Hartmann number *Ha*. Figure 4 influence of Weissenberg number *We* on radial velocity profile. It is noticed that the radial velocity profile reduces with increasing values of Weissenberg number *We*. Physically, deduced as the relaxation time of fluid advances for higher stander of Weissenberg number *We* causing reduction in radial velocity profile. Figure 5 depicts the nature of *We* on azimuthal velocity profile. It is found that an oscillatory pattern encountered for growing values of *We* assist the flow in negative y-direction. Figure 6 illustrates the impact of rotation parameter λ on radial velocity

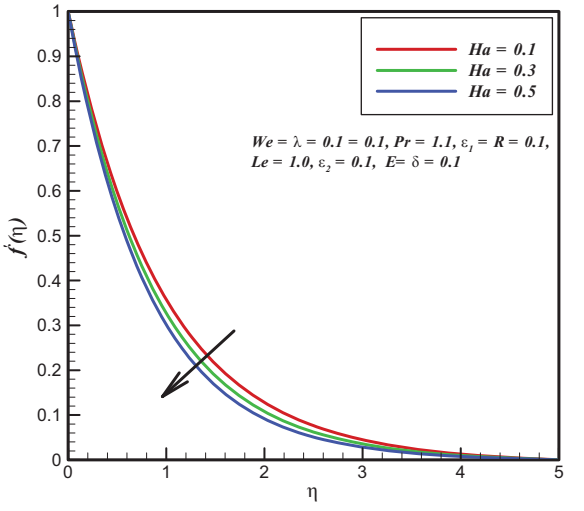

Figure 2.
$f'(\eta)$ against *Ha*

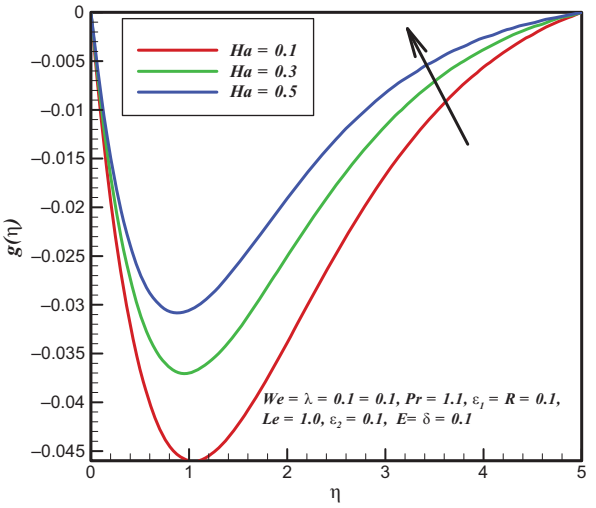

Figure 3.
$g(\eta)$ against Ha

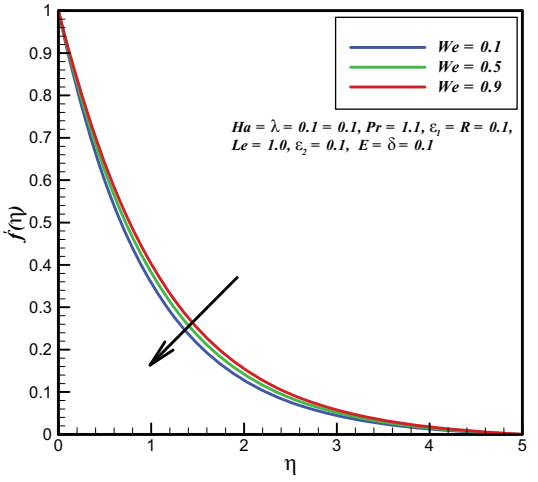

Figure 4.
$f'(\eta)$ against We

profile. It is found that radial velocity increases for large values of λ. For $\lambda = 0$, the frame is non-rotating. With gradually improvement in λ, rotation rate gets stronger than the stretching rate and offer more conflict to the liquid motion. Eventually, a thinner boundary layer with improve in radial velocity profile is observed. Figure 7 influence of rotation parameter λ on azimuthal velocity. It is fact that an oscillatory pattern confront for improving values λ which accommodate the flow is negative direction. Figure 8 is plotted for several values of Prandtl number Pr against temperature profile. In this figure we can analyze that an increment in Pr generates a marked decrease in the temperature distribution. For increasing values of Pr lower thermal diffusivity causes reduction in temperature. Such kind of lower thermal diffusivity signifies the decrement in temperature profile. Figure 9 displays the

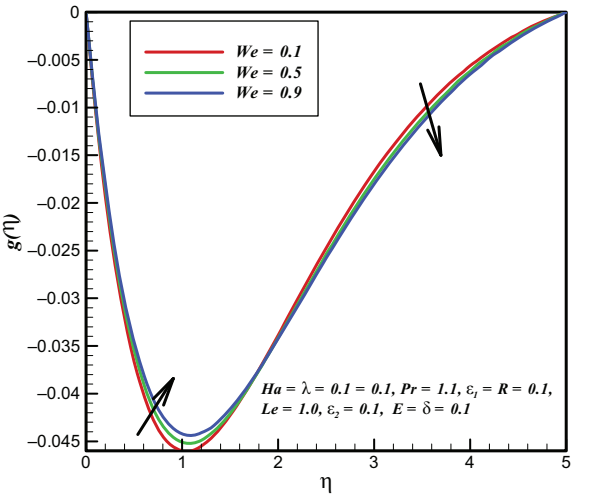

Figure 5.
$g(\eta)$ against We

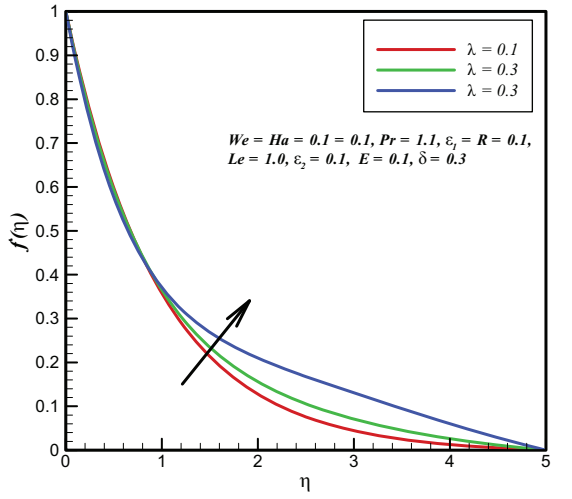

Figure 6.
$f'(\eta)$ against λ

behavior of radiation parameter R on temperature profile. It is found that temperature profile enhances for enhancing values of solar radiation parameter R. This is because an increase in the solar radiation parameter R leads to enhance boundary layer thickness. Figure 10 presents the effect of variable thermal conductivity ε_1 on temperature distribution. It is also clear that the temperature of the liquid for the case of constant thermal conductivity ($\varepsilon_1 = 0$) is less than that of the liquid having variable thermal conductivity i.e, $\varepsilon_1 \neq 0$. Thermal boundary layer thickness enhances when thermal conductivity parameter ε_1 is improved. Figure 11 is plotted to explain the influence of Eckert number Ec on temperature profile. It is noticed that the temperature profile enhances with enhancing Eckert number Ec, this is due to the action of friction heating. For low-speed liquids, the viscous heating can be ignored. Figure 12 presents the effect of concentration diffusion

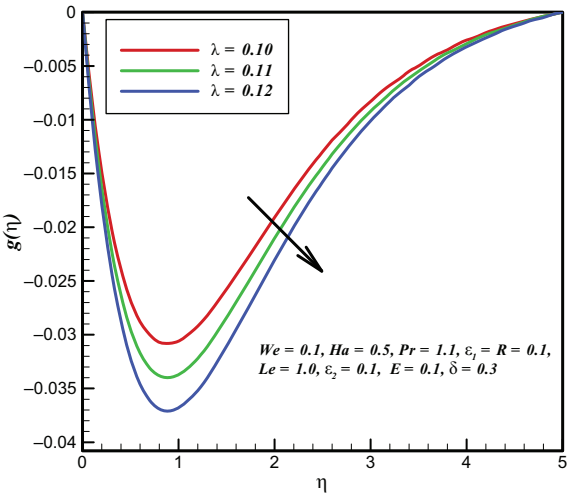

Figure 7.
$g(\eta)$ against λ

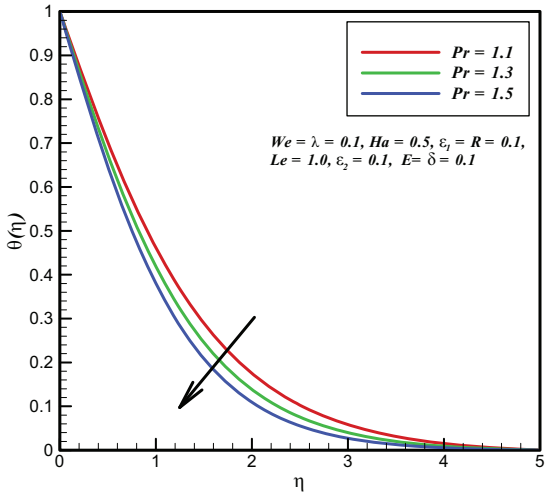

Figure 8.
$\theta(\eta)$ against Pr

coefficient ε_2 on concentration profile. It can be analyzed that concentration diffusion has improving rate under diffusion coefficient. Accordingly, the concentration boundary layer thickness enhances when concentration diffusion coefficient ε_2 is improved. In Figure 13, the behavior of Lewis number Le on concentration distribution has been displayed. It can be examined that the higher values of Lewis number Le reduces the mass concentration. Therefore, the concentration profile reduces by enhancing values of Lewis number Le. Figure 14 is plotted to depict the effect of temperature difference parameter δ on concentration profile. Figure 15 represents the nature of dimensionless activation energy E on concentration profile. Physically, improve in values of activation energy E lower the temperature. Table I gives the numerical

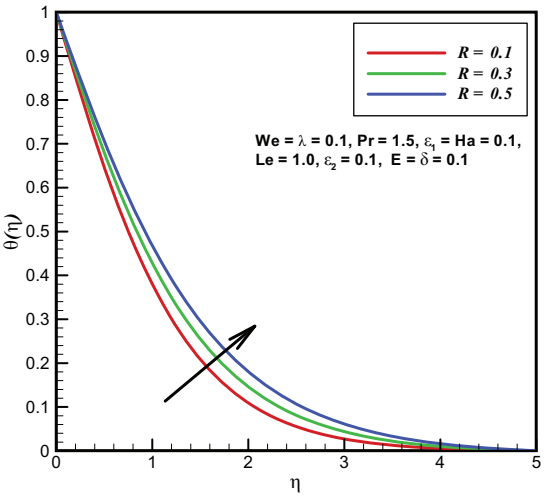

Figure 9.
$\theta(\eta)$ against R

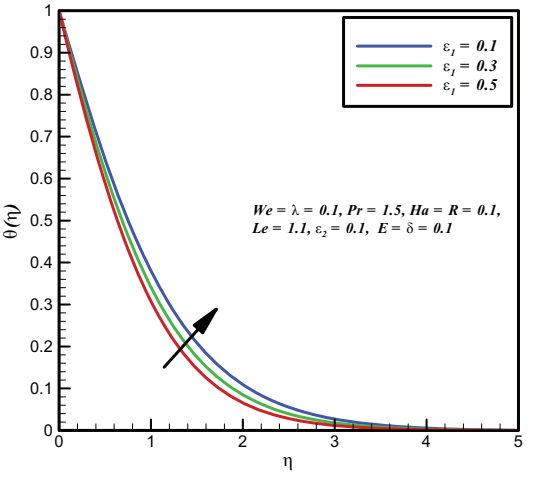

Figure 10.
$\theta(\eta)$ against ε_1

results of skin friction coefficient with respect to behavior of various physical parameters. It is observed that for enhancing values of Hartmann number and rotation parameter, the skin friction coefficient enhances. Moreover, as expected, skin friction coefficient reduces with enhancing values of Weissenberg number *We*. Table II computational values of heat transfer rate with respect to variation of different physical parameters. It can be analyzed that increasing values of Prandtl number Pr, thermal conductivity parameter ε_1 and solar radiation parameter R increases the heat transfer rate. Therefore, as expected, rate of heat transfer reduces with increment values of Eckert number *Ec*. Table III depicts that the concentration diffusion coefficient ε_2 increases the mass transfer rate. This is obvious form the date

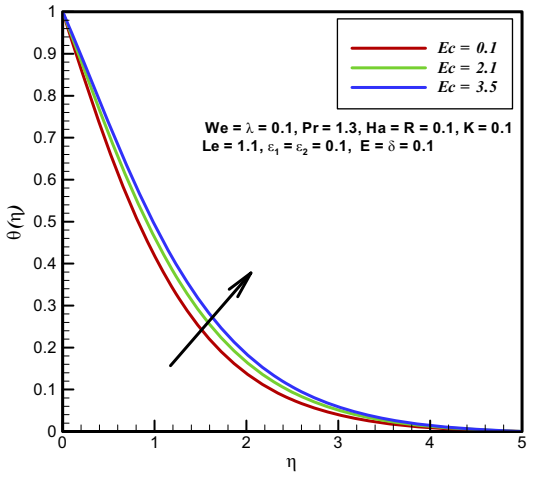

Figure 11.
$\theta(\eta)$ against Ec

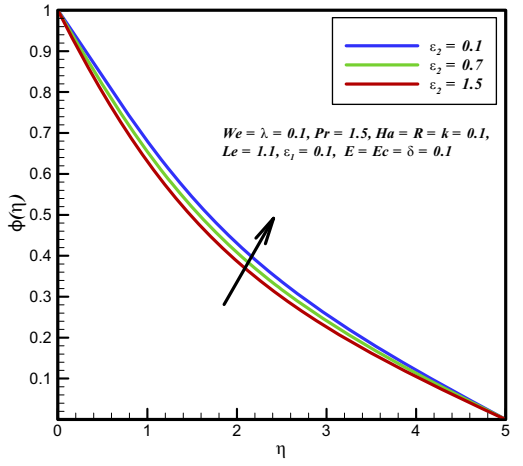

Figure 12.
$\phi(\eta)$ against ε_2

of this table that reduction is noticed for large values of Lewis number *Le*, chemical reaction rate K and dimensional difference rate parameter δ.

5. Concluding remarks

The mathematical model including heat and mass diffusions in Williamson fluid flow along a rotating stretching surface has been analyzed in existence of transverse magnetic field and solar radiation. The numerical solution has been achieved and the effects of several dimensionless parameters on diffusion phenomena have been analyzed. Some of the main points are:

- For increasing values of Hartmann number *Ha* and Weissenberg number, *We* the radial velocity profile reduces. Whereas the converse trend is noticed in the case of *Ha* and *We*.

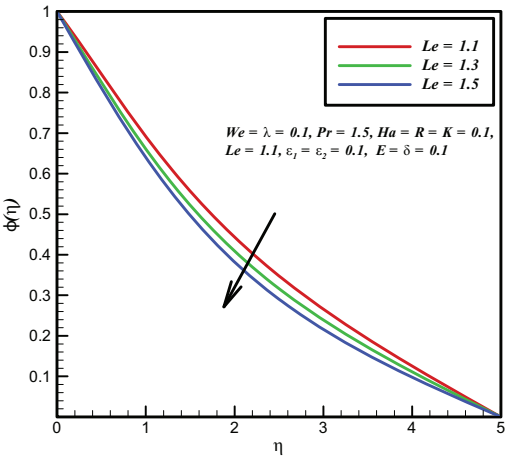

Figure 13.
$\phi(\eta)$ against Le

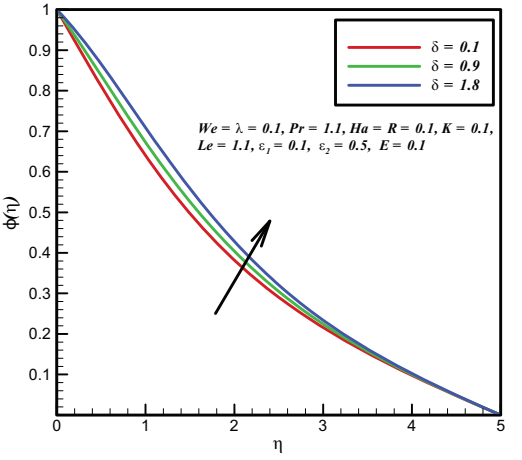

Figure 14.
$\phi(\eta)$ against δ

- It is found that increase in values of rotation parameter λ reduces the radial velocity profile.
- Eckert number Ec and Radiation parameters R have important role in the improvement of heat phenomena.
- Rising values of Prandtl number Pr reduces the temperature distribution. Whereas the opposite trend is noticed for thermal conductivity ε_1.
- Concentration profile enhances for increasing values of concentration diffusion coefficient ε_2, dimensional difference parameter δ and activation energy parameter E.

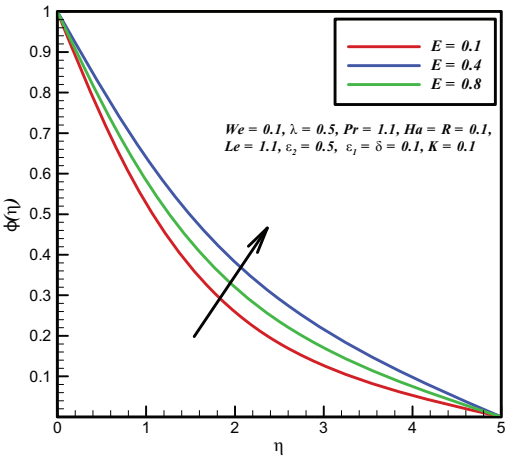

Figure 15. $\phi(\eta)$ against E

Ha	We	λ	$C_{f_x}\mathrm{Re}_x^{\frac{-1}{2}}$	$C_{f_y}\mathrm{Re}_x^{\frac{-1}{2}}$
0.1			1.1275	0.1177
0.3			1.2245	0.1043
0.5			1.3148	0.0944
	0.1		1.1275	0.1177
	0.3		1.0697	0.1151
	0.5		1.0237	0.1131
		0.10	1.1275	0.1177
		0.11	1.1288	0.1299
		0.12	1.1303	0.1422

Table I. Numerical results for wall friction factor $\left(C_f\mathrm{Re}_x^{\frac{1}{2}}\right)$ for unlike values of *Ha*, *We* and λ. When $Le = Pr = 1.1$, $E = \delta = Ec = \mathrm{K} = \varepsilon 1 = \varepsilon 2 = 0.1$

Pr	$\varepsilon 1$	R	Ec	$\mathrm{Nu}\mathrm{Re}_x^{\frac{-1}{2}}$
1.1				−0.6903
1.2				−0.7261
1.3				−0.7610
	0.1			−0.6903
	0.2			−0.7449
	0.3			−0.7933
		0.1		−0.6903
		0.2		−0.7115
		0.3		−0.7323
			0.1	−0.6903
			0.2	−0.6835
			0.3	−0.6772

Table II. Computational results of heat diffusion rate $\left(Nu\mathrm{Re}_x^{\frac{-1}{2}}\right)$ for different values of Pr, ε_1, R and Ec. When $Le = 1.1$, $E = \delta = \lambda = Ha = K = We = \varepsilon 2 = 0.1$

Table III.
Values of mass diffusion rate $\left(Sh\mathrm{Re}_x^{\frac{-1}{2}}\right)$ for unlike values of Le, ε_2, K, E and $Ec = 0.3$. When $Pr = 1.1$, $E = \delta = K = \varepsilon_1 = Ha = \lambda = We = 0.1$

Le	ε_2	K	E	δ	$\mathrm{Sh}\mathrm{Re}_x^{\frac{-1}{2}}$
1.1					−0.3375
1.2					−0.3092
1.3					−0.2750
	0.1				−0.3375
	0.2				−0.3514
	0.3				−0.3641
		0.1			−0.3375
		0.2			- 0.0433
		0.3			- 0.3978
			0.1		−0.3375
			0.2		−0.3742
			0.3		−0.4077
				0.1	−0.3375
				0.2	−0.3572
				0.3	−0.3118

References

Azizian, R., Doroodchi, E., McKrell, T., Buongiorno, J., Hu, L.W. and Moghtaderi, B. (2014), "Effect of magnetic field on laminar convective heat transfer of magnetite nanofluids", *International Journal of Heat and Mass Transfer*, Vol. 64, pp. 94-109.

Chen, X., Ye, Y., Zhang, X. and Zheng, L. (2018), "Lie-group similarity solution and analysis for fractional viscoelastic MHD fluid over a stretching sheet", *Computers and Mathematics with Applications*, Vol. 75, pp. 3002-3011.

Eid, M.R. and Mahny, K.L. (2017), "Unsteady MHD heat and mass transfer of a non-Newtonian nanofluid flow of a two-phase model over a permeable stretching wall with heat generation/absorption", *Advanced Powder Technology*, Vol. 28 No. 11, pp. 3063-3073.

Farooq, A., Ali, R., Ali, S. and Benim, A.C. (2018), "Soret and dufour effects on three dimensional Oldroyd-B fluid", *Physica A*, Vol. 503, pp. 345-354.

Gireesha, B.J., Kumar, K.G., Ramesh, G.K. and Prasannakumara, B.C. (2018), "Nonlinear convective heat and mass transfer of Oldroyd-B nanofluid over a stretching sheet in the presence of uniform heat source/sink", *Results in Physics*, Vol. 9, pp. 1555-1563.

Hayat, T., Ali, S., Farooq, M.A. and Alsaedi, A. (2015), "On comparison of series and numerical solutions for flow of eyring-powell fluid with Newtonian heating and internal heat generation/absorption", *Plos One*, Vol. 10 No. 9, pp. e0129613.

Hayat, T., Ali, S., Awais, M. and Alsaedi, A. (2016a), "Joule heating effects on MHD flow of burgers' fluid", *Heat Transfer Research*, Vol. 47 No. 12, pp. 1083-1092.

Hayat, T., Ali, S., Alsaedi, A. and Alsulami, H.H. (2016b), "Influence of thermal radiation and joule heating in the flow of Eyring-Powell fluid with soret and dufour effects", *Journal of Applied Mechanics and Technical Physics*, Vol. 57 No. 6, pp. 1051-1060.

Jonnadulaa, M., Polarapu, P., Reddy, G. and Venakateswarlu, M. (2015), "Influence of thermal radiation and chemical reaction on MHD flow, heat and mass transfer over a stretching surface", *Procedia Engineering*, Vol. 127, pp. 1315-1322.

Khan, M., Malik, M.Y., Salahuddin, T. and Hussian, A. (2018a), "Heat and mass transfer of williamson nanofluid flow yield by an inclined Lorentz force over a nonlinear stretching sheet", *Results in Physics*, Vol. 8, pp. 862-868.

Khan, M., Shahid, A., Malik, M.Y. and Salahuddin, T. (2018b), "Thermal and concentration diffusion in Jeffery nanofluid flow over an inclined stretching sheet: a generalized Fourier's and Fick's perspective", *Journal of Molecular Liquids*, Vol. 251, pp. 7-14.

Khan, M., Salahuddin, T., Malik, M.Y. and Mallawi, F.O. (2018c), "Change in viscosity of Williamson nanofluid flow due to thermal and solutal stratification", *International Journal of Heat and Mass Transfer*, Vol. 126, pp. 941-948.

Khan, M., Salahuddin, T. and Malik, M.Y. (2018d), "An immediate change in viscosity of Carreau nanofluid due to double stratified medium: application of Fourier's and Fick's laws", *Journal of the Brazilian Society of Mechanical Sciences and Engineering*, Vol. 40 No. 9, p. 457.

Khan, M., Shahid, A., Salahuddin, T., Malik, M.Y. and Mushtaq, M. (2018e), "Heat and mass diffusions for Casson nanofluid flow over a stretching surface with variable viscosity and convective boundary conditions", *Journal of the Brazilian Society of Mechanical Sciences and Engineering*, Vol. 40 No. 11, doi: 10.1007/s40430-018-1415-y.

Khan, M., Malik, M.Y., Salahuddin, T., Rehman, K.U., Naseer, M. and khan, I. (2017), "MHD flow of Williamson nanofluid over a cone and plate with chemically reactive species", *Journal of Molecular Liquids*, Vol. 231, pp. 580-588.

Kumaran, G. and Sandeep, N. (2017), "Thermophoresis and Brownian moment effects on parabolic flow of MHD Casson and Williamson fluids with cross diffusion", *Journal of Molecular Liquids*, Vol. 233, pp. 262-269.

Makinde, O.D., Mabood, F., Khan, W.A. and Tshehla, M.S. (2016), "MHD flow of a variable viscosity nanofluid over a radially stretching convective surface with radiative heat", *Journal of Molecular Liquids*, Vol. 219, pp. 624-630.

Mishra, S.R. and Bhatti, M.M. (2017), "Simultaneous effects of chemical reaction and Ohmic heating with heat and mass transfer over a stretching surface: a numerical study", *Chinese Journal of Chemical Engineering*, Vol. 25 No. 9, pp. 1137-1145.

Nadeem, S., Hussain, S.T. and Lee, C. (2013), "Flow of a Williamson over a stretching sheet", *Brazilian Journal of Chemical Engineering*, Vol. 30 No. 3, pp. 619-625.

Nourazar, S.S., Hatami, M., Ganji, D.D. and Khazayinejad, M. (2017), "Thermal-flow boundary layer analysis of nanofluid over a porous stretching cylinder under the magnetic field effect", *Powder Technology*, Vol. 317, pp. 310-319.

Pal, D. and Mandal, G. (2017), "Double diffusive magnetohydrodynamic heat and mass transfer of nanofluids over a nonlinear stretching/shrinking sheet with viscous-Ohmic dissipation and thermal radiation", *Propulsion and Power Research*, Vol. 6 No. 1, pp. 58-69.

Qureshi, I.H., Nawaz, M., Rana, S. and Zubair, T. (2018), "Galerkien method finite element study on the effect of variable thermal conductivity and variable mass diffusion conductance on heat and mass transfer", *Communication Theoretical Physics*, Vol. 70, pp. 49-50.

Ramay, D., Raju, R.S., Aao, J.A. and Chamkha, A.J. (2018), "Effects of velocity and thermal wall slip on magnetohydrodynamics (MHD) boundary layer viscous flow and heat transfer of a nanofluid over a non-linearly-stretching sheet: a numerical study", *Propulsion and Power Research*, Vol. 7, pp. 182-195.

Sarojamma, G., Lakshmi, R.V., Sreelakshmi, K. and Vajravelu, K. (2018), "Dual stratification effects on double-diffusive convective heat and mass transfer of a sheet-driven micropolar fluid flow", *Journal of King Saud University-Science*, doi: 10.1016/j.jksus.2018.05.027.

Soomro, F.A., Usman, M., Haq, R.U. and Wang, W. (2018), "Thermal and velocity slip effects on MHD mixed convection flow of Williamson nanofluid along a vertical surface: modified legendre wavelets approach", *Physica E: Low-Dimensional Systems and Nanostructures*, doi: 10.1016/j.physe.2018.07.002.

Sreedevi, P., Reddy, P.S. and Chamkha, A.J. (2017), "Heat and mass transfer analysis of nanofluid over linear and non-linear stretching surfaces with thermal radiation and chemical reaction", *Powder Technology*, Vol. 315, pp. 194-204.

Sui, J., Zhao, P., Cheng, Z. and Doi, M. (2018), "Influence of particulate thermophoresis on convection heat and mass transfer in a slip flow of a viscoelasticity-based micropolar fluid", *International Journal of Heat and Mass Transfer*, Vol. 119, pp. 40-51.

Turkyilmazoglu, M. (2018), "Analytical solutions to mixed convection MHD fluid flow induced by a nonlinearly deforming permeable surface", *Communications in Nonlinear Science and Numerical Simulation*, Vol. 63, pp. 373-379.

Williamson, R.V. (1929), "The flow of pseudoplastic materials, industrials and engineering chemistry research", *Industrial and Engineering Chemistry*, Vol. 21, p. 1108.

Corresponding author
Mair Khan can be contacted at: mair.khan@math.qau.edu.pk